Free Radical Biology and Medicine 163 (2021) 234–242

Contents lists available at ScienceDirect

Free Radical Biology and Medicine

journal homepage: www.elsevier.com/locate/freeradbiomed

Original article

pH-dependent rearrangement determines the iron-activation and antitumor activity of artemisinins

Guangcan Bai [1], Yibo Gao [1], Sijin Liu, Sufang Shui, Guoquan Liu [*]

State Key Laboratory of Natural and Biomimetic Drugs, School of Pharmaceutical Sciences, Peking University, Beijing, 100191, China

A B S T R A C T

The action mechanisms of artemisinins remains elusive for decades, and one long-standing question is whether the indispensable peroxide group is activated by iron or heme. Although heme usually reacts faster with artemisinins than iron does, we have found that rearrangement of dihydroartemisinin (DHA) into monoketo-aldehyde-peroxyhemiacetal (MKA) under physiological conditions can significantly enhance its reaction towards iron. The rearrangement is pH-dependent and the derived MKA is identified by LC-MS in the cellular metabolites of DHA in cancer cells. MKA reacts quickly with ferrous irons to afford reactive carbon-centered radicals and can inhibit enzyme activities *in vitro*. Moreover, MKA oxidizes ferrous irons to ferric irons, which may explain the effect of DHA on decreasing cellular labile iron pool (LIP). Both addition of exogenous iron and increase in LIP via triggering ferroptosis can enhance the cytotoxicity of DHA against cancer cells. While artesunate (ATS) can also decompose to MKA after hydrolyzing into DHA, the other artemisinins of lower antitumor activity, e.g. artemisinin (ART), artemether (ATM) and arteether (ATE), exhibit negligible hydrolysis and rearrangement under the same conditions. Our study reveals the vital role of molecular rearrangement to the activation and activity of artemisinins and provides a new strategy for designing antitumor molecules containing endoperoxide group.

1. Introduction

Artemisinins (see Scheme 1), which are extensively used as the first-line antimalarial drug [1–3], have also exhibited potential efficacy in treatment of cancers [4–8]. However, the action mechanism of artemisinins against cancer cells, resembling that against *plasmodium falciparum*, has remained elusive for decades. It is generally agreed that the endoperoxide group of artemisinins is indispensable to maintain the activity [9], but the intermediate radicals generated after activation of the endoperoxide groups complicated the situation. These highly active intermediates could promiscuously target their surrounding molecules, in a fashion differing from the conventional binding mechanism that is usually involved one or a couple of targets [10–13]. Therefore, activation of artemisinins determines dominantly their targets and is the key to understand the action mechanism. But how the endoperoxide group breaks up into radicals is also under debate. While both free ferrous iron and heme can activate artemisinins in solutions drastically deviating from physiological conditions [14–19], the *in vivo* activator is controversial. In cancer cells, it has been speculated that iron is the main activator mainly based on evidences that modulation of intracellular iron level by chelators or exogenous iron could mediate the antitumor efficacy of artemisinins [6,20–22]. In contrast, recent studies based on chemical proteomics using an artemisinin derivative with a labelling tail to trace or pull down binding proteins have recapitulated the role of heme in the activation [23–26]. Following this avenue, mitochondria that is the home to synthesize heme and contains abundant proteins incorporated heme as the active center, have been suggested as the target of artemisinins in cancer cells [27]. Moreover, artemisinins have shown significantly difference in their antitumor efficacy [7,28,29]. DHA and ATS exhibit higher efficacy than the other artemisinins, e.g. ART, ATE and ATM, both *in vivo* and *in vitro*. Although the metabolic transformation into DHA has been identified *in vivo* for these artemisinins to take effects [30–32], the molecular mechanism through which DHA exhibits higher efficacy remains unknown.

Here, we have applied electron paramagnetic resonance (EPR) to monitor the activation of artemisinins under physiological conditions through analyzing the intermediate radicals. We demonstrate the vital effects of molecular rearrangement on the reactivity and efficacy of artemisinins, which have been previously overlooked. The rearrangement occurs both in mild PBS and in cancer cells, and the derived MKA (see Scheme 1) reacts rapidly with ferrous irons and oxidize them into ferric irons. Our observation can explain the ability of artemisinins to induce iron-dependent ferroptosis and the different antitumor activity of these artemisinins.

* Corresponding author.
E-mail address: guoquanliu@bjmu.edu.cn (G. Liu).
[1] These authors contributed equally.

https://doi.org/10.1016/j.freeradbiomed.2020.12.024
Received 17 November 2020; Received in revised form 2 December 2020; Accepted 7 December 2020
Available online 25 December 2020

2. Results

2.1. Artemisinins exhibit different antitumor activity

DHA and ATS distinct from ART, ATM and ATE in their antitumor activity. In the NCI 60 cancer cell lines, DHA exhibits decent activity against most of them with IC_{50} even lower than 20 μM in some cell lines (Fig. 1a). ATS is also active with a slightly higher IC_{50}, but ART, ATM and ATE are not efficient in killing these cancer cells with IC_{50} almost larger than 100 μM. This division has been also observed in several other cell lines (Supplementary Fig. 1a). We further confirmed the different activity of these artemisinins in A549 from the NCI 60 cell lines, and in HT1080. While 200 μM DHA and ATS resulted in significant cell death in both cell lines, ART, ATM and ATE showed negligible effects on cell death assessed by CCK-8 (Fig. 1b and d). Moreover, we examined the effects of modulation of iron and heme on the cytotoxicity. In both cell lines, addition of exogenous iron sensitized cells to DHA and ATS, but not to the other three artemisinins (Fig. 1c, Supplementary Fig. 1c and d). Consistently, the iron chelator deferoxamine (DFO) effectively blocked the cell death (Fig. 1e). According to previous reports, addition of aminolevulinic acid (ALA) or protoporphyrin IX (PPIX, the immediate precursor to heme) could enhance cellular heme level, while application of succinylacetone (SA, an inhibitor of ALA dehydratase) could lower the heme level [24]. Given the definitive ability of heme to react with artemisinins, the inhibition of its synthesis would more realistically reveal its role in activation of artemisinins. In A549, we observed that addition of SA imposed negligible effects on cell death resulted from DHA or ATS (Fig. 1e). In summary, iron, instead of heme, plays a key role in cell deaths caused by DHA and ATS in A549 and HT1080 cells.

2.2. Rearrangement promotes the reaction of DHA and ATS with irons

Both free ferrous iron and hemin activate artemisinins *in vitro*, but it is difficult to make an accurate comparison between their reaction rates under exactly the same conditions. Heme has to be dissolved in alkaline solution, where ferrous iron would be easily oxidized by air. Thus dimethyl sulfoxide (DMSO) mixed with phosphate buffer solution (PBS) of pH = 7.4 was used for heme and actetonitrile (ACN) mixed pure water was used for Fe^{2+} (ratio 2:8), and HPLC was then applied to monitor the decomposition of artemisinins (Table 1). Up to 1 h, all five artemisinins remains nearly unchanged in the presence of ferrous iron and hemin (the oxidized state of heme). To generate heme at its reduced state *in situ*, reductant GSH was added into the hemin solution. All artemisinins reacted almost immediate with heme and disappeared completely within 1 h. Under this condition, artemisinins react more rapidly with heme than with ferrous iron.

To mimic the physiological condition during cell treatment, we firstly incubated artemisinins in cell lysate diluted with Minimum Eagle's medium (MEM, 2 million cells/mL) and thereafter examined their reactivity with irons. The reaction was monitored *in situ* without sample separation through detection of the generated radicals by EPR, owing to the high sensitivity and clean background of this technique. Strikingly, incubation of DHA in cell lysate/MEM dramatically changed its reactivity towards iron (Fig. 2a). The higher EPR signal observed after 2 h-incubation suggested the activation of DHA by forming an intermediate that could react much faster with iron than DHA did. We then analyzed the key factors that changed the activity of DHA. Incubation of DHA or ATS in MEM with/without FBS (fetal bovine serum) had also been examined. The similar reactivity enhancement observed in all three media demonstrated that MEM was sufficient to activate DHA (Fig. 2b) or ATS (Supplementary Fig. 2a), which fortunately simplified the analysis. We next compared the activation of all artemisinins in MEM. In contrast to DHA and ATS were significantly activated, ART, ATM and ATE were still insensitive to iron after 6 h or 12 h incubation (Fig. 2c), interestingly consistent with their division in antitumor activity (Fig. 1).

HPLC was then applied to search the intermediate derivatives of higher reactivity toward irons formed during the decomposition of DHA in MEM. Two dominant peaks of shorter retention time appeared while the remaining DHA was negligible after incubation for 6 h (Fig. 2d). The two new peaks were ascribed to the two epimers of MKA (refer to characterization shown in Supplementary Figs. 3 and 4), the rearrangement derivative of DHA that has been previously reported [33–35]. Because carbonate was used as the buffer to maintain pH in MEM, hours of exposure of MEM (at 37 °C) to air might result in pH changes due to the changing CO_2 content in solution. We therefore investigated the incubation of DHA in PBS to maintain a stable pH. MKA also appeared as the main derivative in the HPLC spectrum of DHA incubated in PBS of pH = 7.4 (Fig. 2d) and its portion dominated during

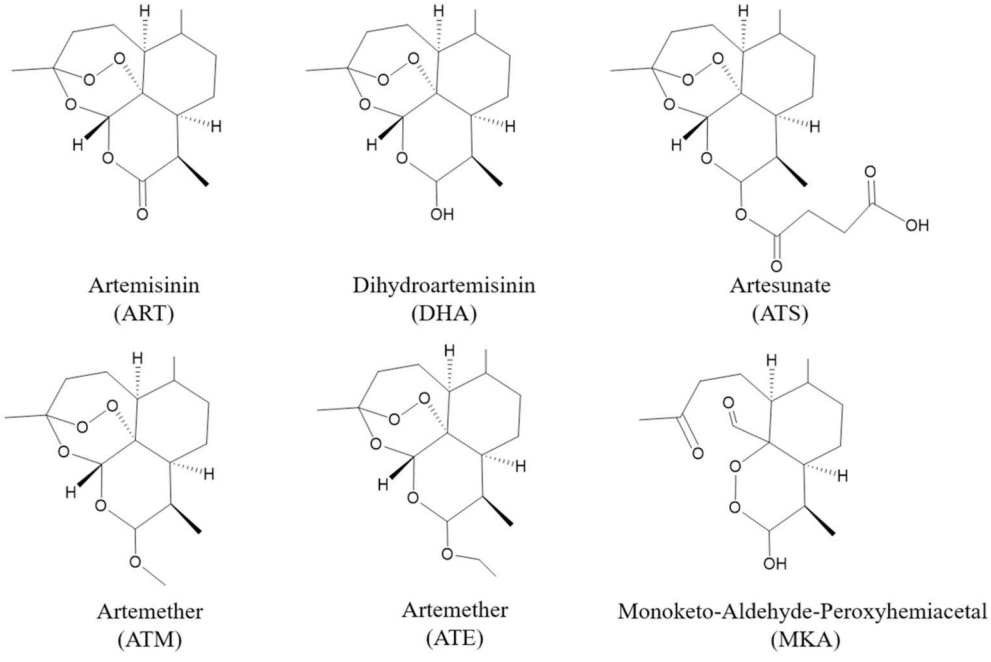

Scheme 1. Chemical structures of artemisinin and its derivatives.

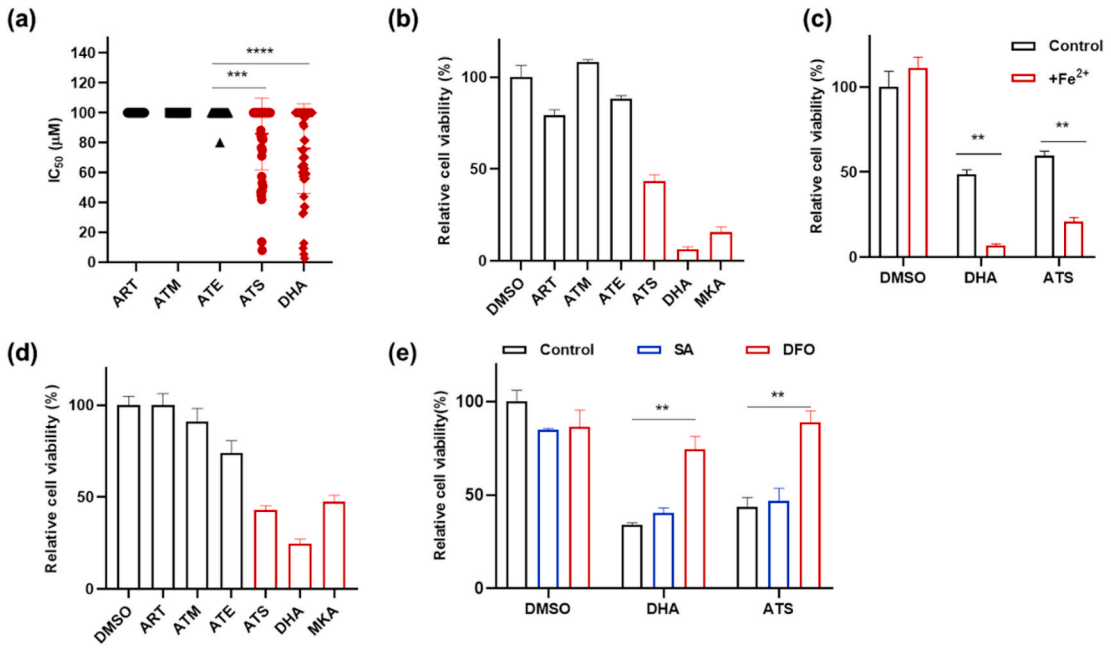

Fig. 1. Cytotoxicity of artemisinins. (a) IC_{50} of artemisinins in NCI 60 cell lines obtained from the NCI database (http://dtp.nci.nih.gov). IC_{50} > 100 μM was all recorded as 100 μM that was the maximum testing concentration. (b) Cytotoxicity of artemisinins (200 μM) in HT1080 cells. (c) Effects of ferrous iron (40 μM) on HT1080 cells treated with DHA or ATS (100 μM). (d) Cytotoxicity of artemisinins (200 μM) in A549 cells. (e) Effects of SA (500 μM) and DFO (100 μM) on A549 cells treated with DHA (100 μM) or ATS (200 μM). The cell viability is measured by CCK-8 after 24 h incubation.

Table 1
Decomposition of artemisinin derivatives by different activators after 1 h incubation. Artemisinin quantity was assessed by peak area in HPLC taking the group with Fe^{2+} just after mixing as 1 and three duplicate experiments were carried out. 200 μM artemisinin was incubated with 200 μM activator at 25 °C in DMSO/PBS (2 : 8) for hemin or ACN/H_2O (2:8) for Fe^{2+}. GSH was 1 mM. ND stands for non-detectible.

	ART	DHA	ATS	ATM	ATE
Fe^{2+}	1.00 ± 0.06	1.01 ± 0.02	0.94 ± 0.08	0.99 ± 0.02	0.92 ± 0.05
Fe^{2+}+GSH	0.98 ± 0.06	1.05 ± 0.08	0.90 ± 0.18	0.98 ± 0.04	0.98 ± 0.03
Hemin	1.05 ± 0.05	1.01 ± 0.06	1.04 ± 0.04	0.96 ± 0.08	0.77 ± 0.09
Hemin + GSH	ND	ND	ND	ND	ND

the decomposition of DHA over time (Fig. 2e).

The as obtained derivative MKA reacted much more quickly with irons than both its parent DHA and the other artemisinins (Fig. 2f). Besides MKA, all the other constituents from the decomposition of DHA afforded negligible EPR signal in the presence of irons. Therefore, MKA is the effective intermediate that changed the reactivity of DHA after incubation in MEM or PBS.

Furthermore, the pH dependence experiments showed that DHA decomposed more rapidly with increasing pH (Fig. 2g) starting from pH = 6.0, consistent with a previous report [35]. In these alkaline solution, MKA was still the main decomposition product of DHA (Supplementary Fig. 2c). Therefore, the higher activation of DHA in MEM than in PBS (Fig. 2b) could be reasonably accounted for by the higher pH in air-exposed MEM than in PBS (pH = 7.4). Moreover, ATS underwent the same rearrangement after its hydrolization into DHA, while both MKA and DHA were observed during its incubation in PBS (Supplemental Fig. 2d and e). At pH = 7.4, the decomposition exhibits a half-life time $t_{1/2}$ of about 6 h for DHA (Fig. 2f), which is much shorter than the usual treatment duration of artemisinins in cancer cells (e.g. 24 h in our experiments). ATS decomposed at a slower rate than DHA did at pH = 7.4 (Fig. 2g) with a smaller portion of MKA present, which is consistent with its lower reactivity towards irons after incubation (Fig. 2c).

2.3. *MKA oxidizes ferrous irons to afford carbon radicals and inhibits enzyme activity*

Although a slightly lower antimalarial efficacy of MKA was reported by Hsien Tao Chi [36], its reactivity and antitumor activity have not yet been clarified. We had observed that MKA reacted more quickly with irons than the other artemisinins (Fig. 2f). MKA afforded immediately a dramatic EPR signal after mixing with irons and dropped over time quickly in the first hour and slowly thereafter. This two-phase feature indicated the presence of at least two radical species of different stability (Supplementary Fig. 9a and b). We therefore used 5,5-Dimethyl-1-pyrroline N-oxide (DMPO) and 2-Methyl-2-nitrosopropane (MNP) as the spin trapping agents to identify the nature of radicals formed after MKA reacted with irons. DMPO can be used to differentiate carbon radicals from oxygen radicals. The fact that we detected only carbon radicals in MKA and dominant hydroxyl radicals in *tert*-Butyl hydroperoxide (*t*-BuOOH) indicated that the endoperoxide ring of MKA was not dissociated into tangling hydropeoxide during reaction with irons (Fig. 3a, Supplementary Fig. 9d). Artemisinins can form both primary and secondary carbon radicals [18], and the former is supposed to react with residues of proteins based on LC-MS analysis [26,37]. However, only EPR evidence of the secondary carbon radical has been reported [18], because the primary carbon radicals were too reactive to be trapped. Using MNP as the spin trapping agent, we obtained for the first time the EPR evidence of the primary carbon radical in artemisinin derived MKA (Fig. 3b). Indeed, the highly reactive primary carbon radical could only be detected with high concentration of MKA and its signal disappeared quickly within several minutes (Supplementary Fig. 9c).

Moreover, MKA, as well as *t*-BuOOH, oxidized ferrous iron into ferric iron based on colorimetric assay (Fig. 3c). In contrast, all artemisinins including DHA and ATS exerted negligible effects on ferrous iron, consistent with their slower reaction rates.

The generation of reactive carbon radicals may reasonably explain

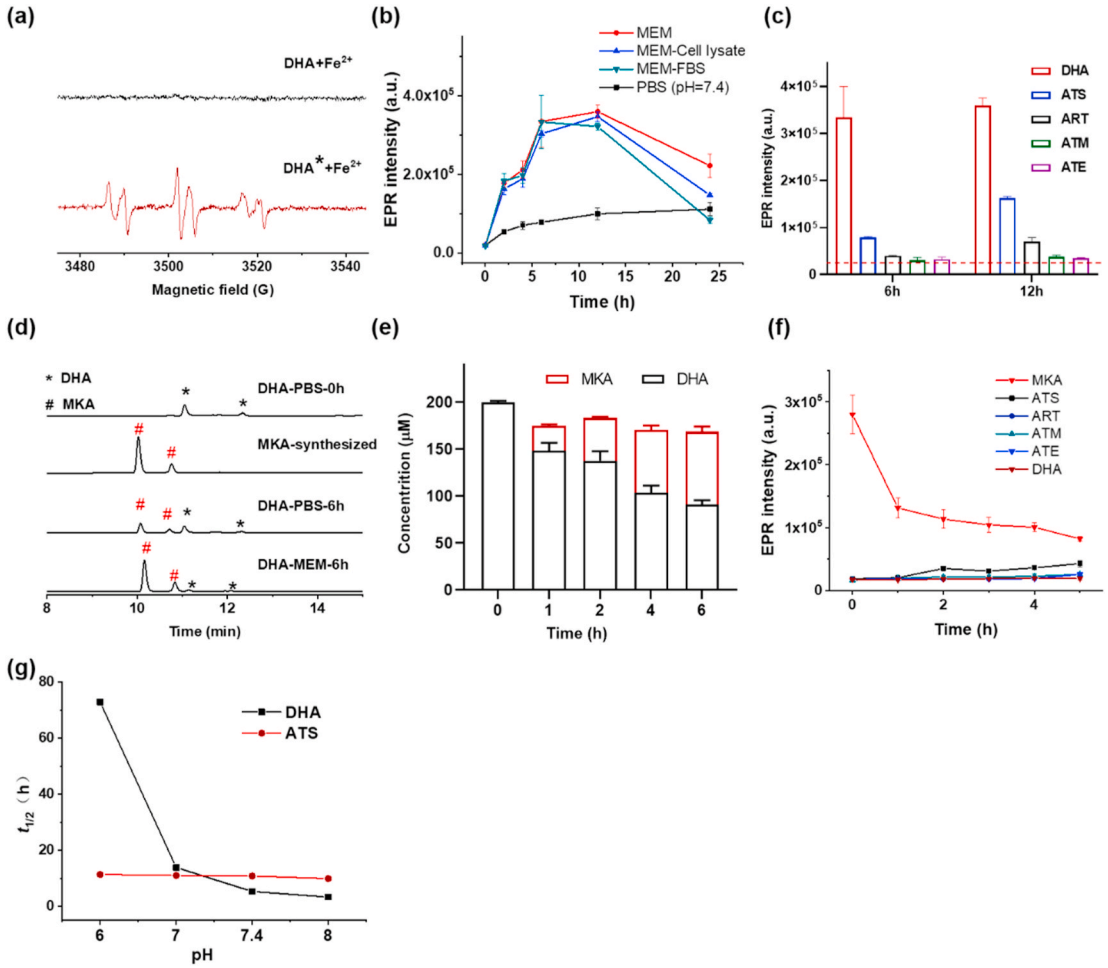

Fig. 2. Incubation in different media affects the reactivity of artemisinins towards irons. (a) EPR spectra of DHA mixed with ferrous irons (1 mM $FeSO_4$). * denotes DHA incubated 2 h in cell lysate (2 million cells/ml in MEM) before the mixing. (b) Evolution of the reactivity of DHA towards ferrous irons after incubation in different media. (c) Comparison of the reactivity of artemisinins towards irons after incubation in MEM for 6 h or 12 h. Red dotted line stands for the signal intensity of the background. (d) Chromatograms of DHA (two epimers) and its rearrangement product MKA (two epimers) in MEM and PBS (pH = 7.4). (e) The concentration evolution of MKA during the decomposition of DHA in PBS (pH = 7.4). (f) Comparison of reactivity towards ferrous irons between MKA and the artemisinins. (g) The pH-dependent decomposition half-life time of DHA and ATS (0.2 mM). In EPR experiments, 1 mM artemisinin dissolved in ACN was incubated in corresponding medium for designated time and then 1 mM $FeSO_4$ was added to check its reactivity towards iron. The radicals formed after the reaction was detected by using α-(4-Pyridyl N-oxide)-N-tert-butylnitrone (POBN) as the spin trapping agent. (For interpretation of the references to color in this figure legend, the reader is referred to the Web version of this article.)

the promiscuous targeting of artemisinins to proteins including some key enzymes [25,26]. However, according to the previous report [25], heme, rather than Fe^{2+}, could activate artemisinins' binding to enzymes and inhibiting their enzyme activities *in vitro*. We therefore examined whether Fe^{2+} could activate MKA to inhibit the activities of enzymes, e.g. lactate dehydrogenase (LDH) and pyruvate kinase (PyrK). Functional assays showed that MKA exhibited dose-dependent enzyme-inhibiting effect on LDH (Fig. 3d) and PyrK (Supplementary Fig. 8a) in the presence of 100 μM ferrous iron. In contrast, DHA, ART, ATM and ATE indeed exhibit negligible inhibitory effect on both LDH and PyrK at 100 μM (Fig. 3e, Supplementary Fig. 8b), which is consistent with the previous report [25] and can be explained by their slower reactivity towards irons (Figs. 2f and 3c). These enzyme-inhibiting results demonstrate the feasibility of MKA acting as the intermediate of DHA and ATS to target proteins in cells.

2.4. DHA metabolizes to MKA in cancer cells

The fact that the rearrangement of DHA occurs at time scale of hours in PBS (pH = 7.4) motivated us to examine the presence of MKA in the cellular metabolites of DHA. Using LC-MS of the multiple reaction monitoring mode (MRM), MKA could be distinguished from its parent DHA (of the same molecular weight) and many other disturbing molecules in the cellular extracts. The two epimers of MKA were clearly identified in the acetonitrile extract of cells lysed after treatment with DHA (Fig. 4a). The concentration of metabolized MKA reached the highest point at 6 h treatment, and thereafter decreased (Fig. 4b). After 24 h treatment with DHA, a significant amount of MKA was still present, which was consistent with the decomposition rate of DHA in PBS of pH = 7.4. The highest concentration at 6 h treatment was estimated to be ~45 μg/mL by comparison its peak area to that of the standard solution.

2.5. MKA, DHA and ATS induce iron-dependent ferroptosis

In both A549 and HT1080 cell lines, the cytotoxicity of MKA lied between DHA and ATS (Fig. 1b and d), and the addition of iron also sensitized cells to MKA (Fig. 5a). The fact that MKA did not exhibit higher activity than DHA is not surprising. Firstly, rearrangement of DHA is fast enough (~6 h at pH = 7.4) to maintain a rapid reaction with iron (Fig. 2g). Secondly, the highly reactive MKA may more likely undergo side reactions before meeting the key targets inside the cells.

Because MKA could quickly oxidize ferrous irons (Fig. 3c), we

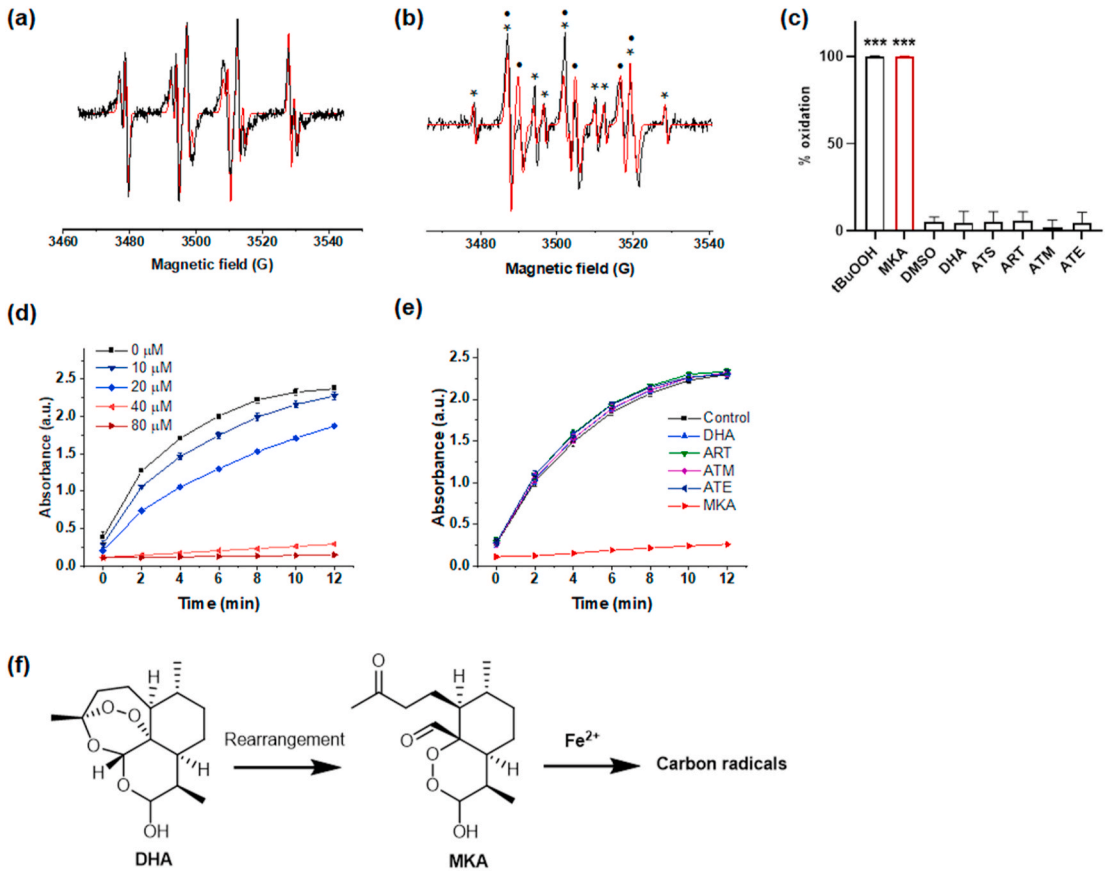

Fig. 3. Reactivity of MKA with ferrous iron and enzymes. (a) EPR spectrum using DMPO (200 mM) of MKA (1 mM) reacted with ferrous irons (1 mM). Two carbon-centered radical species were identified from the simulation. i: $a_N = 15.66$ G, $a_H = 21.08$ G; ii: $a_N = 15.43$ G, $a_H = 18.35$ G. (b) EPR spectrum using MNP (80 mM) of MKA (5 mM) with ferrous ion (2.5 mM). Primary carbon radical (*): $a_N = 15.97$ G, $a_{H\beta} = 9.22$ G ($2H_\beta$); secondary carbon radical (•): $a_N = 15.02$ G, and $a_H = 3.00$ G. (c) Oxidation of ferrous irons (200 μM) in the presence of different oxidizing agents (200 μM). (d) Dose-dependence of the enzyme-inhibiting effect of MKA on LDH in the presence of 100 μM $FeSO_4$. (e) Comparison of the enzyme-inhibiting effect of artemisinins and MKA (100 μM) on LDH in the presence of 100 μM $FeSO_4$. (f) Schematic representation of the rearrangement of DHA into MKA, and the subsequent generation of carbon-centered radicals in the presence of ferrous iron.

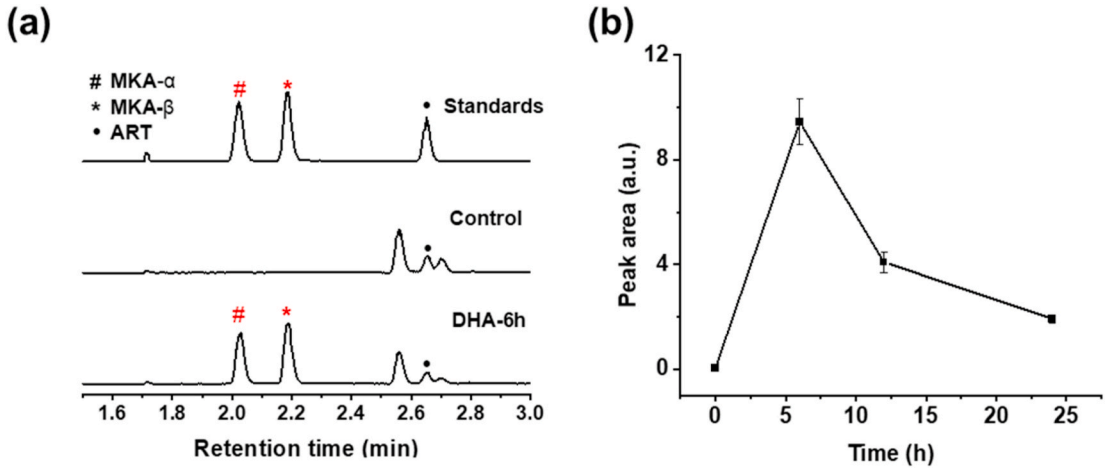

Fig. 4. DHA metabolizes to MKA in cancer cells. (a) LC-MS analysis of metabolized MKA from A549 cells treated with DHA. Both MKA and ART were used as standards in ACN solution. As a control, ART was added to the extract of cells treated with/without DHA. (b) The peak area (in LC-MS) of metabolized MKA at 6, 12 and 24 h after treatment with DHA in A549 cells.

measured the changes in cytosolic iron level in MKA treated cells by calcein AM fluorescence. As expected, MKA significantly reduced the LIP level indicated by an intensity enhancement of the calcein AM fluorescence in the presence of DFO (Fig. 5b), probably due to oxidization of the cellular ferrous irons into ferric irons. Interestingly, DHA also reduced the LIP level (Fig. 5b), suggesting that it indeed undergo rearrangement to form MKA in cancer cells. ATS, as well as other artemisinins, did not decrease the cellular LIP level, probably due to its lower MKA level resulting from the slower decomposition rate (Fig. 2g). The ability of DHA to decrease the LIP level explains the fact artemisinins

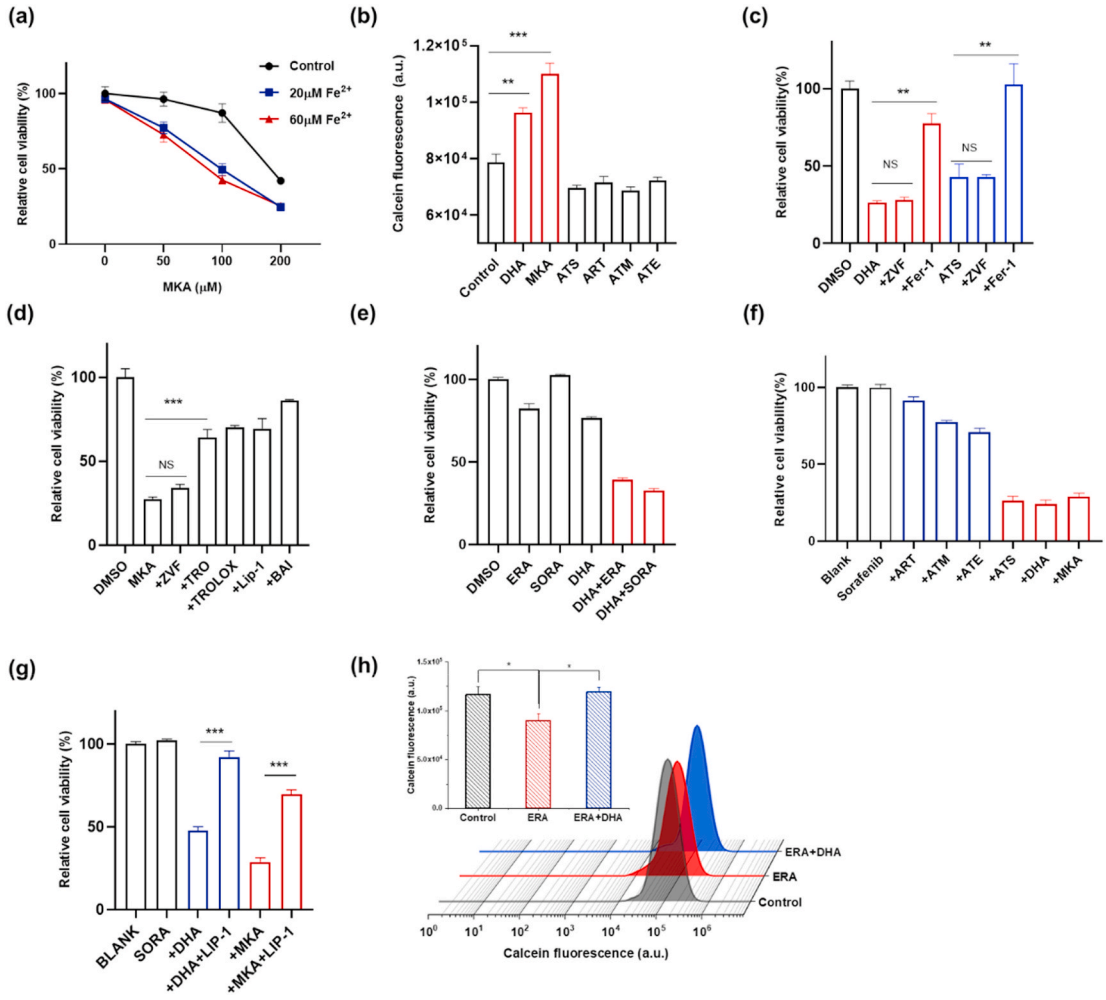

Fig. 5. MKA and artemisinins induce ferroptosis. (a) Fe^{2+} enhanced the cytotoxicity of MKA in A549 cells. (b) DHA and MKA significantly decreased the LIP level measured by calcein-AM (in the presence of 100 μM DFO) in HT1080 cells. DHA/ATS/MKA 40 μM, and ART/ATM/ATE 200 μM. (c) DHA and ATS (200 μM) induced ferroptosis in A549 cells. ZVF 25 μM, Fer-1 12.5 μM. (d) MKA (200 μM) induced ferroptosis in HT1080 cells. ZVF 25 μM, Lip-1 6 μM, BAI 3 μM, TRO 3 μM, TROLOX 3 μM. (e) Erastin (ERA, 2 μM) or Sorafenib (SORA, 5 μM) enhanced the cytotoxicity of DHA (50 μM) in HT1080 cells. (f) Cytotoxicity comparison of artemisinins and MKA when co-treated with Sorafenib (5 μM). ATS/DHA/MKA 100 μM, ART/ATM/ATE 200 μM. (g) Cytotoxicity resulted from co-treatment of Sorafenib (5 μM) with DHA or MKA (100 μM) could be blocked by Lip-1 (6 μM). (h) DHA (20 μM) reduced the increased LIP level caused by erastin (1 μM) in HT1080 cells.

could regulate iron homeostasis reported previously [28,29].

It has been reported that artemisinins can induce iron-dependent ferroptosis [28,29], which was also confirmed in both A549 and HT1080 cells (Fig. 5c). While the pan-caspase inhibitor Z-VAD-fmk (ZVF) did not significantly prevent the cell death induced by DHA and ATS, the typical ferroptosis inhibitor Ferrostatin-1 (Fer-1) prevented the majority of cell death. Mitochondrial was previously reported to be a target of artemisinins in both yeast and some cancer cells, whose damage usually lead to cell apoptosis [11,38]. We measured the mitochondria membrane potential (MMP) and found no changes up to a concentration of 40 μM, a feature consistent with ferroptosis instead of apoptosis (Supplementary Fig. 10). Consistently, cell death induced by MKA followed the similar pathway with DHA and ATS, where typical ferroptosis inhibitors, e.g. Liproxstatin-1 (LIP-1) [39], effectively prevented the cell death (Fig. 5d).

Because increase in LIP level is one of the hallmarks of ferroptosis, this advantage could be taken to facilitate the activation of DHA and ATS and enhance their anticancer activity. The ferroptosis inducer erastin, or antitumor drug Sorafenib that may also induce ferroptosis in some cases [40,41], was treated together with artemisinins. As shown in Fig. 5e, both erastin and Sorafenib could enhance the cytotoxicity of DHA. Expectedly, the sensitizing effects of Sorafenib were more evident in DHA, ATS and MKA than in ART, ATM and ATE (Fig. 5f), a division consistent with their difference in cytotoxicity and rearrangement ability. All cell deaths in the combination treatment of Sorafenib with either DHA or MKA, were efficiently inhibited by Lip-1 (Fig. 5g), indicating they converged on the ferroptosis pathway. Moreover, the LIP measurements showed that DHA could restore the increased iron level in both erastin or Sorafenib treated cells to a normal level (Fig. 5h, Supplementary Fig. 11), consistent with its ability to decrease LIP level when used alone (Fig. 5b). In summary, all MKA, DHA and ATS induce ferroptotic cell death and exhibit syngeneic effects with other ferroptosis inducers, e.g. erastin and Sorafenib.

3. Discussion

Although the activation of artemisinins by ferrous iron was slow, we have discovered that molecular rearrangement can dramatically enhance the reactivity of DHA and ATS towards ferrous irons (Fig. 2c). The rearrangement derivative MKA has been previously obtained under harsh conditions, e.g. strong acid [36], pyrolysis [33], strong alkaline [34]. After examining a series of media to mimic the physiological conditions, pH has been identified as the key factor affecting rearrangement. The assistance of N-benzyldihydronicotinamide (a model

compound of NADH) used in a previous report [42] was not essential, but it could accelerate the process because of its alkaline. The half-life time of decomposition of DHA is about 6 h in PBS of pH = 7.4 (Fig. 2g), which is compatible with the time scale to exert its efficacy in cells. Moreover, MKA has been identified for the first time, to our best knowledge, in the metabolites of DHA in cells (Fig. 4), which strongly suggests its important role in the action mechanism of artemisinins.

MKA reacts rapidly with ferrous irons to generate reactive carbon radicals and exhibits enzyme-inhibiting effects (Fig. 3). Especially, MKA can oxidize ferrous irons into ferric irons. Such an iron oxidation has also been previously reported for FINO2, a ferroptosis inducer with an endoperoxide group [43]. Accordingly, DHA, as well as MKA, could decrease the cellular LIP level in cancer cells probably through oxidizing ferrous irons into ferric irons. Our results are consistent with a previous observation that DHA increased IRP-IRE affinity to enhance iron importing, in contrast to the ferroptosis inducer erastin [28].

The rearrangement into MKA can explain the difference of antitumor activity among artemisinins. DHA and ATS exhibiting higher antitumor activity could be quickly rearranged under physiological conditions. A previous study in NCI 60 cancer lines has shown that their response to artemisinins correlates with iron-related genes and hierarchical cluster analysis reveals two different groups of artemisinins [29]. Interestingly, DHA and ATS are different from ATM, ATE and ART in that cluster analysis, consistent with their division in rearrangement behavior (Fig. 2c).

Over the longstanding argument on the iron source in the activation of artemisinins, the role of rearrangement has been neglected. The recent chemical proteomics approach demonstrates that heme rather than ferrous iron can activate artemisinin derivatives *in vitro*, in cancer cells and in plasmodium parasite [25,26]. These proofs are evident but their inference to other artemisinins has to be taken cautiously, especially in cancer cells. Artemisinin derivatives used in these studies were designed with labelling groups for tracing or pulling down proteins, which blocks the effective rearrangement of these derivatives into MKA. Therefore, the observation that only heme can activate these derivatives does not exclude the possibility of iron-activation of DHA and ATS as observed in our studies. Multiple factors, e.g. cell lines, doses may complicate the situation in cancer cells. The proofs that heme modulation could mediate the cytotoxicity of DHA and ATS are difficult to explain the antitumor activity difference among artemisinins, while all the five artemisinins we studied react rapidly with heme (Table 1). To reconcile the conflicting conclusions, we propose that iron and heme simultaneously activate artemisinins in cancer cells, and the one that dominates cell death may vary with cell lines and the nature of functionalized groups attached to artemisinins. Some artemisinins indeed concentrate in mitochondria, especially those with a targeting group like TPP, and cause apoptosis probably through damaging the mitochondria [27]. Others, especially DHA and ATS, can undergo rearrangement and react mainly with ferrous irons without specifically targeting the mitochondrial, and result in ferroptosis via influencing the iron hemostasis or oxidizing poly unsaturated fatty acids (PUFA).

The rearrangement mainly accounts for the syngeneic effects of artemisinins with erastin and Sorafenib, through utilizing the increased LIP in ferroptotic cell deaths (Fig. 5e). This would shed light on using artemisinins in combination with other chemotherapies, especially ferroptosis inducers, which has already been demonstrated in mouse models [28]. The generally well-tolerated artemisinins may further sensitize cells to ferroptosis and improve the therapeutic effects. Moreover, the rearrangement of DHA to MKA also inspires novel design strategies of peroxide-containing compounds by coupling the activation to factors promoting rearrangement, e.g. microenvironment pH or hydrolysis enzymes, to improve their antitumor targeting and activity.

4. Conclusions

To conclude, rearrangement under physiological conditions sensitizes DHA and ATS to ferrous irons through the intermediate MKA, which rapidly oxidizes ferrous irons to ferric irons and effectively inhibits enzyme activities. Both MKA and DHA decrease the LIP level in cancer cells. Moreover, all MKA, DHA and ATS result in ferroptotic death in A549 and HT1080 cells, and act synergistically with other ferroptosis inducers through utilizing the enhanced LIP level. Our studies demonstrate that the rearrangement potential of artemisinins is consistent with their cytotoxicity and is therefore vital to understanding the iron source in the activation of artemisinins.

5. Experimental method

5.1. Materials

Artemisinin (ART), artemether (ATM), artemether (ATE), dihydroartemisinin (DHA), artesunate (ATS) were purchased from DeSiTe (Chengdu DeSITe Biological Technology Co.,Ltd). K_2HPO_4, KH_2PO_4, Hemin, GSH, Ferrostatin-1(Fer-1), Liproxstatin-1(Lip-1), Baicalein (BAI), Trolox, troglitazone (TRO), CA-074 methyl ester, Z-VAD-fmk (ZVF) were purchased from Selleck Chemicals LLC. 2-methyl-2nitrosopropane (MNP), FerroZine, Dimethyl-1-pyrroline N-oxide (DMPO), α-(4-Pyridyl N-oxide)-N-tert-butylnitrone (POBN), Deferoxamine (DFO) was purchased from Sigma (St Louis, MO, USA). Succinylacetone(SA) was purchased from Cayman. Sorafenib was purchased from Targetmol. TMRE test kit was purchased form Bestbio. Iron (II) sulfate heptahydrate was purchased from Macklin. Dulbecco's modified Eagle medium (DMEM), Minimum Eagle's medium (MEM), LDH and PyrK assay kits were purchased from Solarbio (Beijing Solarbio Science & Technology Co., Ltd.). *t*-BuOOH was purchased from Energy Chemical.

5.2. Cell culture

A549 cells and HT1080 cells were purchased from the National Infrastructure of Cell Line Resource (China) and have been tested to be negative for mycopasma contamination. Cells were cultured in a 37 °C incubator with 5% CO_2. A549 cells were cultured in the Dulbecco's modified Eagle medium (DMEM) with 10% FBS, 100 U ml^{-1} penicillin, 100 μg ml^{-1} streptomycin (all from M&C GENE TECHNOLOGY (BEIJING) LTD.). HT1080 cells were similarly cultured except using the Minimum Eagle's medium (MEM).

5.3. Cytotoxicity assay

Cells were seeded in 96 well plates (NEST) at a density of 5000 cells per well in 100 μl overnight. The cells were then exposed to artemisinins or other chemicals as specified in different experiments for 24 h. Cell viability were accessed by CCK-8. IC_{50} were calculated using the GraphPad Prism 8 software.

5.4. Measurement of labile iron pool

HT1080 cells were seeds in 24 well plates at a density of 50,000 cells per well in 1 mL overnight. Then cells were treated with artemisinin derivatives or together with regulators. Trypsinized cells were washed twice with PBS and incubated with 0.05 μM calcein-acetoxymethyl ester for 10 min at 37 °C. Cells were then washed twice with PBS and incubated either with DFO (100 μM) for 1 h at 37 °C. Cells were analyzed using a flow cytometer (Beckman CytoFlex). Calcein was excited at 488 nm, and fluorescence was measured at 525 nm. The mean cellular fluorescence with DFO incubation and the amount of LIP are in negative correlation.

5.5. Measurement of MMP

A549 cells were seeded in 24 well plates (NEST) at a density of 50,000 cells per well in 1 mL overnight. Then cells were stained with

artemisinin derivatives for 6 h or 24 h. Cells were washed with PBS and stained with TMRE (BestBio) for 15 min. Then cells were detected in flow cytometry. The data was processed using Graphpad Prism 8.

5.6. Synthesis of MKA

MKA was synthesized following the procedures of a previous report [34]. 35 mg of DHA was added to 5 mL of a ACN/H_2O (70:30) mixture. NaOH was then added (final concentration 2 mM), and the reaction was finished after 1.5 h. The mixture was diluted with water (5 mL), extracted with CH_2Cl_2 (3 × 6 mL), dried over anhydrous Na_2SO_4, and concentrated in vacuum. ~15 mg crude product was obtained. The crude product was further purified by reverse phase HPLC with a semi-preparative Agilent C18 column equilibrated at 25 °C. HPLC solvents comprised of solvent A (0.1% TFA in MilliQ water) and solvent B (0.1% TFA in acetonitrile). A linear gradient from 50 to 95% solvent B was employed in 30 min. Purified MKA was obtained as a pale-yellow oil mixture of two epimers (~2:1); ^{1}H NMR (major epimer) δ = 0.58 (d, 3H), 0.86 (d, 3H, 14-Me), 1.2–1.4 (m, 1H), 1.6–1.8 (m, 2H), 2.05 (s, 3H), 2.3–2.5 (m, 2H), 7.02 (d, 1H),10.19 (s, 1H, CHO); ^{1}H NMR (minor epimer) δ = 0.56 (d, 3H), 0.86 (d, 3H, 14-Me), 1.2–1.4 (m, 1H), 1.6–1.8 (m, 2H), 2.05 (s, 3H), 2.3–2.5 (m, 2H), 7.56 (d, 1H), 10.07 (s, 1H, CHO) (Supplementary Fig. 7); liquid chromatography–mass spectrometry (LC–MS; ESI) calcd. for $[M+H]^+$: 285.1657, found: 285.1705. (Supplementary Fig. 8).

5.7. Colorimetric iron oxidation

In a clear 96-well plate, 5 μL of a 4 mM DMSO solution of test compound and 5 μL of a 4 mM FeSO4 was added to 85 μL of a 2:1 (v/v) solution of water and DMSO. This mixture was incubated at 37 °C for 2 h. 5 μL of a 10 mM stock of FerroZine (Sigma Aldrich) was added. Absorbance was measured at 567 nm.

5.8. LDH inhibition assay

The assay followed the manufacturer's protocol. LDH (1 μg) was first incubated with ferrous sulfate (100 μM) and different concentrations of MKA (0–80 μM) in normal saline (50 μl) at 37 °C for 10min. For comparison of the enzyme-inhibiting effect of artemisinins and MKA the concentration was 100 μM. The resulting mixture was transferred to a 96-well plate, followed by the addition of the reaction buffer (50 μl). LDH activity was subsequently measured by absorbance at 490 nm with microplate reader. The reactions with no LDH added and with LDH without inhibitor served as negative and positive controls, respectively. All measurements were carried out in triplicate.

5.9. Pyruvate kinase inhibition assay

The assay followed the manufacturer's protocol. PyrK (1 μg) was first incubated with ferrous sulfate (100 μM) and different concentrations of MKA (0–80 μM) in normal saline (50 μl) at 37 °C for 10min. . For comparison of the enzyme-inhibiting effect of artemisinins and MKA the concentration was 100 μM. The resulting mixture was transferred to a 96-well plate, followed by the addition of the reaction buffer (50 μl). PyrK activity was subsequently measured by absorbance at 340 nm with microplate reader. The reactions with no PyrK added and with PyrK without inhibitor served as negative and positive controls, respectively. All measurements were carried out in triplicate.

5.10. Detection of MKA in A549 cells

Liquid chromatography–mass spectrometry (LC-MS) was applied to detect the MKA in cells after treatment of 100 μM DHA at 6, 12 and 24 h. HPLC was performed using an Waters ACQUITY QSM (Waters Corp., Milford, USA). The HPLC system was coupled to an XEVO triple-quadrupole mass spectrometer via an electrospray ionization (ESI) interface for mass analysis and detection. Chromatographic separation was achieved on an Acquity UPLC® BEH C18 column (2.1 × 50 mm, 1.7 μm; Waters Corp., Milford, USA). Security Guard C18 (5 μm) guard column (Waters Corp., Milford, USA). The chromatography was performed at room temperature. The mobile phase consisted of A:water containing ammonium formate(5 mM) and 0.1% (v/v) formic acid; B: acetonitrile. 0min, 75%A; 2min, 25%A; 4min, 0%A; 5.5min, 75%A. Flow rate was 0.4 mL/min. The mass spectrometer was operated in positive ion mode. The fragmentation transitions for the multiple reactions monitoring (MRM) were *m/z* 302.0 to 193.0 for MKA. For sample preparation, A549 cells were incubated with DHA in DMEM medium before lysis. Cell lysate was collected and then extracted with 5 vol of acetonitrile. After centrifugation the supernatant was air dried and resolved by 50% acetonitrile before injection and chromatographic analysis.

5.11. Spin-trapping and EPR measurement

Detection of carbon-centered radicals of MKA was performed using MNP or DMPO or POBN as the spin trapping agent. In experiments with MNP, MKA (5 mM), ferrous ion (2.5 mM) and MNP (80 mM) were mixed (ACN/H_2O = 1:1). In experiments with DMPO, MKA (1 mM), ferrous ion (1 mM) and DMPO (200 mM) were mixed (ACN/H_2O = 1:1). In experiments with POBN, MKA (1 mM), ferrous ion (1 mM) and POBN (200 mM) were mixed (ACN/H_2O = 1:1). The samples were measured after vortex immediately and 50 μL aliquots were aspirated in glass capillaries and transferred in the resonator of the EPR spectrometer.

Measurement of the signal intensity of artemisinins reacted with ferrous ion was performed using POBN as the spin trapping agent. Artemisinins (1 mM) was incubation in the corresponding medium (cell lysate, MEM with or without FBS, PBS. All contains 20% ACN) for designated time and the ferrous iron (1 mM), POBN (200 mM) were admixed. Samples were measured after vortex immediately. 50 μL aliquots were aspirated in glass capillaries and transferred in the resonator of the EPR spectrometer.

The EPR spectra were taken at room temperature with an X-band Bruker A200 or E580 spectrometer. Following parameters was used unless otherwise specified: Sweep field range 100 G, sweep time 60 s; modulation amplitude 1 G; modulation frequency 100 kHz, and microwave power 19.23 mW. Simulation of the spectra was done using the EasySpin package [44].

5.12. Measurement of artemisinin decomposition in the presence of activators by HPLC

Artemisinins (200 μM) were mixed with ferrous ion (200 μM) in a final solution of ACN/water (ratio 2:8). For hemin (200 μM), the solution was a mixture of ACN and PBS (ratio 2:8, pH = 7.4). To generate heme at its reduced state *in situ*, reductant GSH (1 mM) was added into the hemin solution. The samples were mixed vigorously after addition of all compounds, and incubated for 0 h or 1 h at 25 °C. After filtration with microfiltration membrane, 1 mL of sample was transferred to HPLC vials.

5.13. Measurement of the pH-dependent decomposition of DHA/ATS by HPLC

Phosphate Buffer Solution (PBS) of different pH (6, 7, 7.4, 8) were prepared at a constant total buffer species concentration of 0.1 M. Sample solutions of DHA at 200 μM were prepared by using 200 μL DHA/ATS stock solution (1 mM in ACN) in a final volume of 2 mL achieved by adding buffer (preheated to 37 °C). The resulting mixture was sealed to prevent water evaporation and maintained at 37 °C.

HPLC measurements were carried out on a Waters Alliance 2695 separations module equipped with a Waters 996 PDA detector.

Empower (V.4.1) software was used for data acquisition. For HPLC measurements the following conditions were used: 20 μL of the respective sample was injected into a column (ZORBAX SB-C18,250 × 4.6 mm, 5 μm, 1 mL/min) and separated using the following gradient: Solvent A was ACN, and solvent B was ultrapure water containing 0.1% phosphoric acid. The applied gradient was as follows: 0–10 min: 5%A-95% A; 10–15 min: 95%A-95%A; 15–20min: 95%A-5%A; 20–22min: 5% A-95%A. UV detector:210 nm; sampling rate: 1000 ms.

5.14. Statistical analysis

Results are expressed as mean ± SD for the indicated number of experiments. Statistical analyses were calculated with Student's t-test. A value of P under 0.05 was considered to be statistically significant.

Acknowledgement

This research is financially supported by the National Natural Science Foundation of China (31971173). We thank Dr. Feng Li for helpful discussions.

Appendix A. Supplementary data

Supplementary data to this article can be found online at https://doi.org/10.1016/j.freeradbiomed.2020.12.024.

References

[1] R.T. Eastman, D.A. Fidock, Artemisinin-based combination therapies: a vital tool in efforts to eliminate malaria, Nat. Rev. Microbiol. 7 (12) (2009) 864–874.
[2] R.W.v.d. Pluijm, et al., Triple artemisinin-based combination therapies versus artemisinin-based combination therapies for uncomplicated Plasmodium falciparum malaria: a multicentre, open-label, randomised clinical trial, Lancet 395 (10233) (2020) 1345–1360.
[3] J. Wang, et al., A temporizing solution to "artemisinin resistance", N. Engl. J. Med. 380 (22) (2019) 2087–2089.
[4] W. Gao, et al., Artemisinin induces A549 cell apoptosis dominantly via a reactive oxygen species-mediated amplification activation loop among caspase-9, -8 and -3, Apoptosis 18 (10) (2013) 1201–1213.
[5] A.L. Greenshields, T.G. Shepherd, D.W. Hoskin, Contribution of reactive oxygen species to ovarian cancer cell growth arrest and killing by the anti-malarial drug artesunate, Mol. Carcinog. 56 (1) (2017) 75–93.
[6] X.-J. Huang, et al., Dihydroartemisinin exerts cytotoxic effects and inhibits hypoxia inducible factor-1alpha activation in C6 glioma cells, J. Pharm. Pharmacol. 59 (6) (2008) 849–856.
[7] X. Li, et al., The selectivity of artemisinin-based drugs on human lung normal and cancer cells, Environ. Toxicol. Pharmacol. 57 (2018) 86–94.
[8] R. Lin, et al., Dihydroartemisinin (DHA) induces ferroptosis and causes cell cycle arrest in head and neck carcinoma cells, Canc. Lett. 381 (1) (2016) 165–175.
[9] S. Kamchonwongpaisan, S.R. Meshnick, The mode of action of the antimalarial artemisinin and its erivatives, Gen. Pharmacol. 27 (4) (1996) 587–592.
[10] U. Eckstein-Ludwig, et al., Artemisinins target the SERCA of Plasmodium falciparum, Nature 424 (6951) (2003) 957–961.
[11] J. Wang, et al., Artemisinin directly targets malarial mitochondria through its specific mitochondrial activation, PloS One 5 (3) (2010), e9582.
[12] S. Zhang, G.S. Gerhard, Heme mediates cytotoxicity from artemisinin and serves as a general anti-proliferation target, PloS One 4 (10) (2009), e7472.
[13] J. Bhisutthibhan, et al., The Plasmodium falciparum translationally controlled tumor protein homolog and its reaction with the antimalarial drug artemisinin, J. Biol. Chem. 273 (26) (1998) 16192–16198.
[14] M. Asano, H. Iwahashi, Determination of the structures of radicals formed in the reaction of antimalarial drug artemisinin with ferrous ions, Eur. J. Med. Chem. 127 (2017) 740–747.
[15] Dr Anne Robert, J.C. Dr, B.M. Dr, Characterization of the alkylation product of heme by the antimalarial drug artemisinin, Angew. Chem. Int. Ed. 40 (10) (2001) 1954–1957.
[16] L. Heller, P.D. Roepe, A.C.d. Dios, Artesunate activation by heme in an aqueous medium, Inorg. Chim. Acta. 496 (2019) 119029.
[17] A. Robert, Y. Coppel, B. Meunier, Alkylation of heme by the antimalarial drug artemisinin, Chem. Commun. (5) (2002) 414–415.
[18] W. Wm, et al., Unified mechanistic framework for the Fe(II)-induced cleavage of qinghaosu and derivatives/analogues. The first spin-trapping evidence for the previously postulated secondary C-4 radical, J. Am. Chem. Soc. 120 (14) (1998) 3316–3325.
[19] S. Zhang, G.S. Gerhard, Heme activates artemisinin more efficiently than hemin, inorganic iron, or hemoglobin, Bioorg. Med. Chem. 16 (16) (2008) 7853–7861.
[20] P.A. Stocks, et al., Evidence for a common non-heme chelatable-iron-dependent activation mechanism for semisynthetic and synthetic endoperoxide antimalarial drugs, Angew. Chem. Int. Ed. 46 (33) (2007) 6278–6283.
[21] T. Efferth, et al., Enhancement of cytotoxicity of artemisinins toward cancer cells by ferrous iron, Free Radic. Biol. Med. 37 (7) (2004) 998–1009.
[22] S.R. Meshnick, et al., Iron-dependent free-radical generation from the antimalarial agent artemisinin (qinghaosu), Antimicrob. Agents Chemother. 37 (5) (1993) 1108–1114.
[23] H.M. Ismail, et al., Artemisinin activity-based probes identify multiple molecular targets within the asexual stage of the malaria parasites Plasmodium falciparum 3D7, Proc. Natl. Acad. Sci. U. S. A 113 (8) (2016) 2080–2085.
[24] W. J, et al., Mechanistic investigation of the specific anticancer property of artemisinin and its combination with aminolevulinic acid for enhanced anticolorectal cancer activity, ACS Cent. Sci. 3 (7) (2017) 743–750.
[25] J. Wang, et al., Haem-activated promiscuous targeting of artemisinin in Plasmodium falciparum, Nat. Commun. 6 (2015), 10111.
[26] Y. Zhou, W. Li, Y. Xiao, Profiling of multiple targets of artemisinin activated by hemin in cancer cell proteome, ACS Chem. Biol. 11 (4) (2016) 882–888.
[27] C.-J. Zhang, et al., Mechanism-guided design and synthesis of a mitochondria-targeting artemisinin analogue with enhanced anticancer activity, Angew. Chem. Int. Ed. 55 (44) (2016) 13770–13774.
[28] G.-Q. Chen, et al., Artemisinin compounds sensitize cancer cells to ferroptosis by regulating iron homeostasis, Cell Death Differ. 27 (2020) 242–254.
[29] E. Ooko, et al., Artemisinin derivatives induce iron-dependent cell death (ferroptosis) in tumor cells, Phytomedicine 22 (11) (2015) 1045–1054.
[30] J.A. Simpson, et al., Population pharmacokinetics of artesunate and dihydroartemisinin following intra-rectal dosing of artesunate in malaria patients, PLoS Med. 3 (11) (2006), e444.
[31] D. T, et al., Comparison of in vitro/in vivo blood distribution and pharmacokinetics of artemisinin, artemether and dihydroartemisinin in rats, J. Pharmaceut. Biomed. Anal. 162 (2019) 140–148.
[32] V. Sinou, et al., Pharmacokinetics of artesunate in the domestic pig, J. Antimicrob. Chemother. 62 (3) (2008) 566–574.
[33] R. Haynes, et al., Artesunate and dihydroartemisinin(DHA):Unusual decomposition products formed under mild conditions and comments on the fitness of DHA as an antimalarial drug, ChemMedChem 2 (10) (2007) 1448–1463.
[34] D. Kotoni, et al., Thermodynamic and kinetic investigation of monoketo-aldehyde-peroxyhemiacetal (MKA), a stereolabile degradation product of dihydroartemisinin, RSC Adv. 4 (62) (2014) 32847–32857.
[35] S. Parapini, et al., Stability of the antimalarial drug dihydroartemisinin under physiologically relevant conditions: implications for clinical treatment and pharmacokinetic and in vitro assays, Antimicrob. Agents Chemother. 59 (7) (2015) 4046–4052.
[36] J.K. Baker, J.D. McChesney, H.T. Chi, Decomposition OF arteether IN simulated stomach acid yielding compounds retaining antimalarial activity, Pharmaceut. Res. 10 (5) (1993) 662–666.
[37] W.C. Li, et al., Characterization of the artemisinin binding site for translationally controlled tumor protein (TCTP) by bioorthogonal click chemistry, Bioconjugate Chem. 27 (12) (2016) 2828–2833.
[38] A. Laleve, et al., Artemisinin and its derivatives target mitochondrial c-type cytochromes in yeast and human cells, Biochim. Biophys. Acta Mol. Cell Res. 1867 (5) (2020) 118661.
[39] O.a. Zilka, R.a Shah, B.a Li, Friedmann Angeli, J.P. b, M.a Griesser, M.b Conrad, D. A. Pratt, On the mechanism of cytoprotection by ferrostatin-1 and liproxstatin-1 and the role of lipid peroxidation in ferroptotic cell death, ACS Cent. Sci. 3 (3) (2017) 232–243.
[40] S. Dolma, et al., Identification of genotype-selective antitumor agents using synthetic lethal chemical screening in engineered human tumor cells, Canc. Cell 3 (3) (2003) 285–296.
[41] E. Lachaier, et al., Sorafenib induces ferroptosis in human cancer cell lines originating from different solid tumors, Anticancer Res. 34 (11) (2014) 6417–6422.
[42] R.K. Haynes, et al., Facile oxidation of leucomethylene blue and dihydroflavins by artemisinins: relationship with flavoenzyme function and antimalarial mechanism of action, ChemMedChem 5 (8) (2010) 1282–1299.
[43] G. Mm, et al., FINO2 initiates ferroptosis through GPX4 inactivation and iron oxidation, Nat. Chem. Biol. 14 (5) (2018) 507–515.
[44] S. Stoll, A. Schweiger, EasySpin, a comprehensive software package for spectral simulation and analysis in EPR, J. Magn. Reson. 178 (1) (2006) 42–55.